optica

All-fiber multiplexed source of high-purity single photons: supplementary material

ROBERT J.A. FRANCIS-JONES*, ROWAN A. HOGGARTH, AND PETER J. MOSLEY

Centre for Photonics and Photonic Materials, Department of Physics, University of Bath, Bath, BA2 7AY, UK
**Corresponding author: r.j.a.francis-jones@bath.ac.uk*

Published 28 October 2016

This document provides supplementary information to "All-fiber multiplexed source of high-purity single photons," http://dx.doi.org/10.1364/optica.3.001270. We present further details of PCF dispersion engineering for factorable photon pair generation, our photonic bandgap fiber wavelength isolation, the characterization of the joint spectral intensity using stimulated emission tomography, and additional information about our calculations of coincidence-to-accidental ratios and second-order coherence.

http://dx.doi.org/10.1364/optica.3.001270.s001

1. PCF DISPERSION ENGINEERING

PCF gives the ability to tune group-velocity dispersion through control of the fiber cladding. We designed and fabricated a PCF with two zero dispersion wavelengths as seen in Fig. S1a and S1c. The resulting phasematching contours, the loci of points with zero phase mismatch between the pump, signal and idler are shown in Fig. S1b. The two ZDWs give phasematching contours that form a pair of closed loops, one for the signal and one for the idler.

In order to generate heralded single photons directly in pure states, correlation must be engineered out of the photon-pair joint spectrum to yield a factorable state $f(\omega_s,\omega_i) = f_s(\omega_s)f_i(\omega_i)$. Two effects contribute to correlation in the JSA, as shown in Fig. S2. Energy conservation results in anti-correlation through the pump envelope function $\alpha(\omega_s+\omega_i)$, and momentum conservation is described by the phasematching function $\phi(\omega_s,\omega_i)$ which is dependent on the dispersion of the medium. The JSA is given by the product of these two functions :$f(\omega_s,\omega_i) = \alpha(\omega_s+\omega_i)\phi(\omega_s,\omega_i)$. Hence by orientating the phasematching function such that the correlation it imparts on the JSA completely counters the contribution of the pump envelope, we can produce a two-photon state in which there are no spectral correlations. In practice this can be achieved by setting the group velocity of the pump to be between that of the signal and the idler [1, 2].

The closed loop phasematching contour means that factorability will always be satisfied for a certain range of pump wavelengths, but the phasematched signal and idler

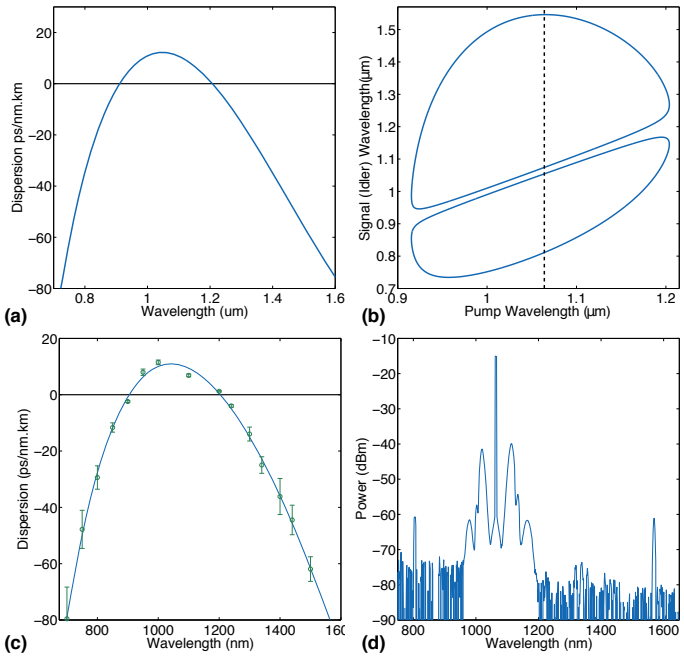

Fig. S1. (a) Target group-velocity dispersion and (b) FWM phasematching plot. (c) Group-velocity dispersion measured by white-light interferometry. (d) Bright FWM spectrum of PCF pumped with sub-nanosecond microchip laser.

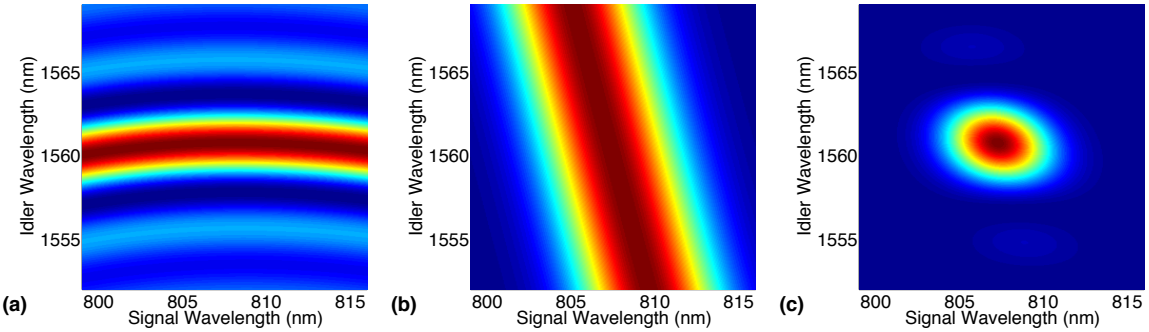

Fig. S2. (a) Simulated phasematching function $\phi(\omega_s, \omega_i)$. (b) Simulated pump envelope function $\alpha(\omega_s + \omega_i)$. (c) Simulated joint spectral intensity $|f(\omega_s, \omega_i|^2$.

wavelengths may not be ideal. Nevertheless, through careful design the PCF structure can be tuned to achieve minimal correlation for a set of target FWM wavelengths, in this case 800 nm and 1550 nm. We have targeted a state where the signal becomes group-velocity matched to the pump. In this case the signal photon is localised to the pump temporal mode, whereas the idler photon walks off from the pump, yielding a narrower bandwidth idler photon. This corresponds to the phasematching function lying parallel to the signal axis in Fig. S2a, when the bandwidths of the phasematching function and pump envelope function are matched, the JSI depicted in Fig. S2c is formed.

During the fiber drawing process, the fabricated fiber was characterised with bright FWM using a 1064nm nanosecond pulsed microchip laser to confirm the wavelength of phasematched FWM. An example FWM spectrum is shown in Fig. S1b. The fiber draw parameters were then adjusted to tune the FWM peaks to the target wavelengths. In Fig. S1b the outer-sideband phasematched solutions at 800 nm and 1550 nm can be clearly seen. Closer to the pump, cascaded FWM can be seen as a result of inner-sideband phasematching; these inner-sideband processes are one source of noise that our PBGF filters had to be capable of removing.

2. PHOTONIC BANDGAP FIBER WAVELENGTH ISOLATION

Due to the large pitch required to form a transmission band at 1550 nm, the mode-field diameter of PBGF-1550 was approximately twice that of SMF-28. Hence a direct splice would have had very high loss due to poor mode overlap between the fibers. To reduce the loss, and also improve the mechanical strength of the splice between PBGF-1550 and SMF-28, tapered-fiber transitions were fabricated using the flame-brush technique [3]. A graded-index large mode area (LMA) fiber was fabricated in which the guided mode and the outer diameter were both matched to that of PBGF-1550 to ensure low loss and high mechanical strength when spliced. The LMA fiber was tapered to a diameter of 125um to match that of SMF-28 whilst also providing good mode overlap. A schematic of the complete spliced PBGF-1550 filter is shown in Fig. S3a. The fundamental mode entering from the SMF-28 was adiabatically transformed in the up-taper region and then launched into the PBGF-1550, and a second down-taper on the output side transformed the mode back to match that of SMF-28 [4]. The transmission through the complete filter shown in Fig. S3b was

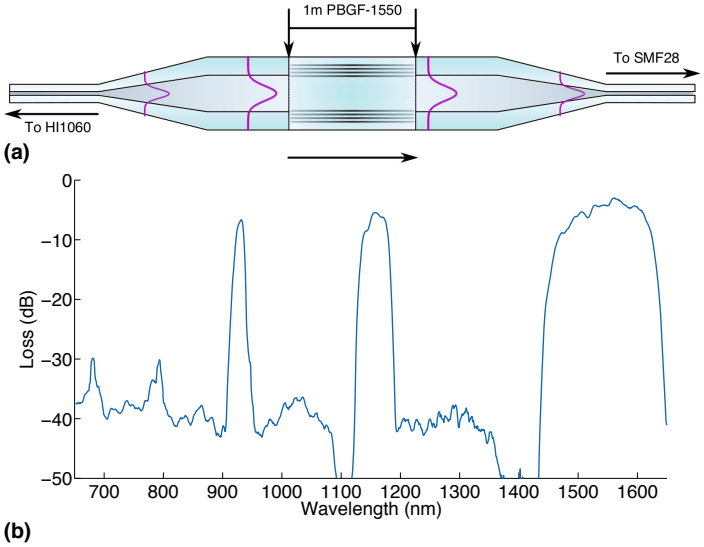

Fig. S3. (a) Schematic of filter with taper transitions.
(b) Transmission through completed PBGF-1550 Filter.

measured by performing a cut-back measurement to yield a loss of ∼2.8 dB at 1550 nm.

3. STIMULATED EMISSION TOMOGRAPHY OF THE JOINT SPECTRAL DENSITY

The FWM joint spectral density was measured by stimulating the process with a seed laser at one of the daughter wavelengths, following the method proposed by Sipe and Liscidini known as stimulated emission tomography [5]. As the spontaneous and stimulated forms of the nonlinear optical interaction are governed by the same phasematching and energy conservation, the stimulated signal is proportional to the probability amplitude of the two photon state.

Each setting of the seed wavelength gave one stimulated signal spectrum as seen Fig. S4. By stacking these spectra the joint spectrum was recovered. The measurement can be made in a short time and at high resolution using an optical spectrum analyser rather than photon-counting detectors.

Figure S5 illustrates the results for a single length of PCF at three different pump wavelengths. The bandwidths of the signal and idler photons are not equal as in this instance the bandwidth of the phasematching function (set by the fiber

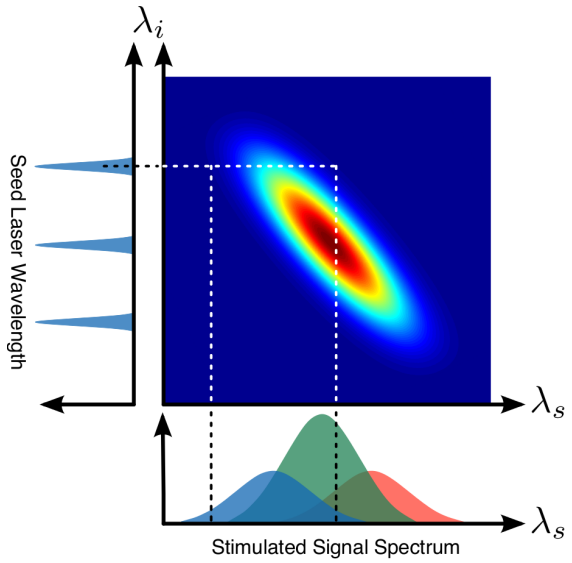

Fig. S4. Stimulated emission tomography measurement.

length) is not well-matched to that of the pump function. Together these three plots may be used to infer the orientation of the phasematching function. As the pump wavelength is tuned, the phasematched signal wavelength increases without a commensurate increase in the idler wavelength. This indicates that the phasematching function lies parallel to the signal axis. This is in agreement with our earlier simulation of the phasematching contours where the resulting signal photon was group-velocity matched to the pump.

4. COINCIDENCE-TO-ACCIDENTALS RATIO

. The coincidence-to-accidental ratio for a single source, $\mathrm{CAR}^{(1)}$, was calculated by taking the ratio of the measured coincidence count rate, $N_c^{(1)}$, to the accidental coincidence rate, $A_c^{(1)}$:

$$\mathrm{CAR}^{(1)} = \frac{N_c^{(1)}}{A_c^{(1)}} = \frac{R_p N_c^{(1)}}{N_H^{(1)} N_I^{(1)}}, \tag{S1}$$

where $N_H^{(1)}$ and $N_I^{(1)}$ are the single count rates in the herald and idler arms respectively and R_p is the repetition rate of the laser.

To calculate the coincidence-to-accidental ratio for our multiplexed source, $\mathrm{CAR}^{(2)}$, we first found the total number of distinct coincidence counts per second, $N_c^{(2)}$, and the total accidentals count rate $A_c^{(2)}$,

$$N_c^{(2)} = N_{H_1 I} + N_{H_2 I} - N_{H_1 H_2 I}, \tag{S2}$$

$$A_c^{(2)} = \frac{N_{H_1} N_I}{R_p} + \frac{N_{H_2} N_I}{R_p} - \frac{N_{H_1} N_{H_2} N_I}{R_p^2}, \tag{S3}$$

The subtraction of the third term on the RHS prevents the double counting of events when both sources produce a heralding signal, but the heralded photon from source 1 is blocked at the switch. The two source $\mathrm{CAR}^{(2)}$ is then,

$$\mathrm{CAR}^{(2)} = \frac{N_c^{(2)}}{A_c^{(2)}}. \tag{S4}$$

5. SECOND ORDER COHERENCE FUNCTIONS

To measure the second-order coherence functions of the idler photons from each source, a 50:50 fiber coupler was incorporated after the switch and in-line polariser, and an additional InGaAs detector monitored the second output of the fiber coupler. The two detectors were gated by the pump laser train and synchronised. The coincidence count rate was measured with an integration time of between 15 and 45 mins. From the raw coincidence count rates we evaluated the marginal second-order coherence function,

$$g_m^{(2)}(0) = \frac{N_{I_1 I_2} \cdot R_p}{N_{I_1} \cdot N_{I_2}}, \tag{S5}$$

or heralded second-order coherence

$$g_H^{(2)}(0) = \frac{N_{H I_1 I_2} \cdot N_H}{N_{H I_1} \cdot N_{H I_2}}. \tag{S6}$$

Note that for all figures in this manuscript no background subtraction has been carried out.

6. LOSS MANAGEMENT

Table S1 details the loss of the constituent components in the source. The use of bespoke fibre for FWM and broadband wavelength isolation, as well as the creation of low-loss tapered interconnects, has enabled us to limit loss in a fully guided-wave architecture. Nevertheless, opportunities exist to reduce loss further through additional engineering. The three crucial areas to target in future systems are: splice loss between the PCF and SMF, loss through the photonic bandgap fibre filters, and switch loss.

Loss in the PCF-to-SMF splice arises from a mismatch in the mode profiles of the two fibres. However, the modes can be better matched by changing the hole size in the PCF cladding during splicing through repeated discharging of the splicing arc to soften the glass and allow the holes to collapse. This technique has been demonstrated in Refs. [6–8] where a loss as low as 0.4 dB was achieved between PCF and SMF at 1550 nm.

We have been able able to reduce the splice loss between SMF and the PBGF filters by incorporating a tapered mode horn made from a graded-index large-mode-area fibre. By moving to large-mode-area fibre with a step-index profile, our simulations show that a higher level of mode overlap should be possible (circa 95% compared to 75% in the current implementation). Hence, including the transmission loss of the PBGF, a total loss of 1 dB could be achieved for a complete filter assembly.

It is crucial that the switch loss be as low as possible to extract the maximum benefit of multiplexing. For the switch used here the loss is 0.94 dB, but this could be reduced further by improvements in the manufacturing process and through the use of anti-reflection coatings in the packaging. Additionally, once the polarisation state of the idler photons from the two sources have been overlapped using the polarisation controllers the polariser could be removed, eliminating an additional 0.6 dB of loss from the system.

Finally, the remaining components (WDMs and FBGs) are technologically mature, therefore there may be not be great potential for reducing the already low loss of the these components further. Overall, with the scope of the potential improvements outlined above, we estimate that the loss in each

Table S1. Table detailing the loss of the constituent components and the potential for further loss reduction.

Component	Loss (dB)		Projected
	800 nm	1550 nm	Loss (dB)
PCF - SMF	2.2	2.0	0.5
WDM	0.4	0.1	<0.1
3× FBG	0.3	0.3	0.3
PBG Filter	2.5	2.8	1
Additional Splices	0.2	0.2	0.2
Polariser	-	0.61	-
Switch	-	0.94	0.5
Total	5.6	6.95	2.6

arm of the source could be reduced to around 2.1 dB at 800 nm and 2.6 dB at 1550 nm.

REFERENCES

1. W. P. Grice, A. B. U'Ren, and I. A. Walmsley, "Eliminating frequency and space-time correlations in multiphoton states," Phys. Rev. A **64**, 063815 (2001).
2. K. Garay-Palmett, H. J. McGuinness, O. Cohen, J. S. Lundeen, R. Rangel-Rojo, A. B. U'ren, M. G. Raymer, C. J. McKinstrie, S. Radic, and I. A. Walmsley, "Photon pair-state preparation with tailored spectral properties by spontaneous four-wave mixing in photonic-crystal fiber," Opt. Express **15**, 14870–14886 (2007).
3. T. Birks and Y. Li, "The shape of fiber tapers," Lightwave Technology, Journal of **10**, 432–438 (1992).
4. J. Love and W. Henry, "Quantifying loss minimisation in single-mode fibre tapers," Electronics Letters **22**, 912–914 (1986).
5. M. Liscidini and J. E. Sipe, "Stimulated emission tomography," Phys. Rev. Lett. **111**, 193602 (2013).
6. L. Xiao, W. Jin, and M. S. Demokan, "Fusion splicing small-core photonic crystal fibers and single-mode fibers by repeated arc discharges," Opt. Lett. **32**(2), 115–117 (2007).
7. X. Zhou, Z. Chen, H. Chen, and J. Hou, "Fusion splicing small-core photonic crystal fibers and single-mode fibers by controlled air hole collapse," Optics Communications **285**(24), 5283 - 5286 (2012).
8. T. Zhu, F. Xiao, L. Xu, M. Liu, M. Deng, and K. S. Chiang, "Pressure-assisted low-loss fusion splicing between photonic crystal fiber and single-mode fiber," Opt. Express **20**(22), 24465–24471 (2012).

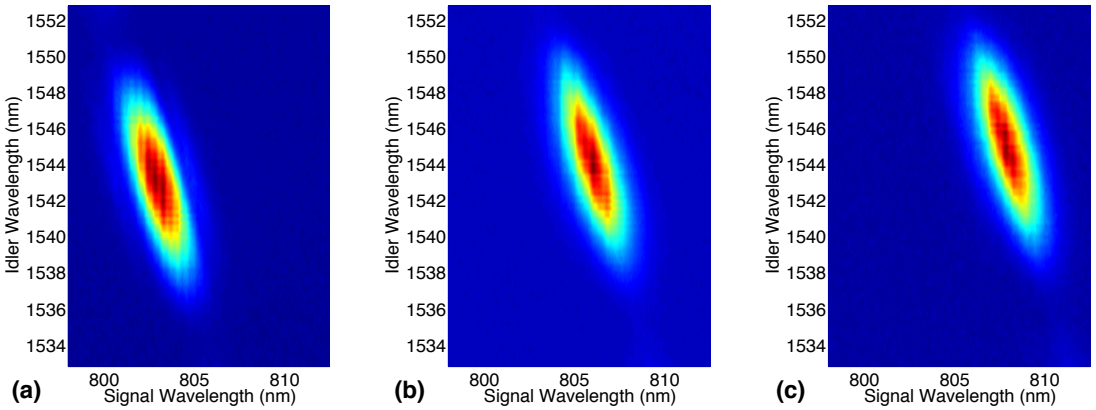

Fig. S5. (a–c) Joint spectrum measured for three pump wavelengths: $\lambda_p = 1057$ nm (left), $\lambda_p = 1059$ nm (middle) and $\lambda_p = 1061$ nm (right).

.